# Coupling of Prolyl Peptide Bond Isomerization and $Ca^{2+}$ Binding in a C-type Mannose-Binding Protein†

Kenneth K.-S. Ng and William I. Weis*

*Department of Structural Biology, Stanford University School of Medicine, Stanford, California 94305*

*Received August 17, 1998; Revised Manuscript Received October 16, 1998*

ABSTRACT: A proline residue flanked by two polar residues is a highly conserved sequence motif in the $Ca^{2+}$- and carbohydrate-binding site of C-type animal lectins. Crystal structures of several C-type lectins have shown that the two flanking residues are only observed to act as $Ca^{2+}$ ligands when the peptide bond preceding the proline residue is in the cis conformation. In contrast, structures of the apo- and one-ion forms of mannose-binding proteins (MBPs) reveal that, when the $Ca^{2+}$-binding site is empty, the peptide bond preceding the proline can adopt either the cis or trans conformation, and distinct structures in adjacent regions are associated with the two proline isomers. In this work, measurements of $Ca^{2+}$-induced changes in intrinsic tryptophan fluorescence, and fluorescence energy transfer from tryptophan to $Tb^{3+}$, reveal a slow conformational change in rat liver MBP (MBP-C) accompanying the binding of either $Ca^{2+}$ or $Tb^{3+}$. The $Ca^{2+}$-induced increase in intrinsic tryptophan fluorescence shows biphasic kinetics: a burst phase with a rate constant greater than 1 $s^{-1}$ is followed by a slow phase with a single-exponential rate constant ranging from 0.01 to 0.05 $s^{-1}$ (36 °C) that depends on the concentration of $Ca^{2+}$. Likewise, addition of EGTA to $Ca^{2+}$-bound or $Tb^{3+}$-bound MBP-C causes a decrease in intrinsic tryptophan fluorescence with biphasic kinetics consisting of a burst phase with a rate constant greater than 1 $s^{-1}$, followed by a slow phase with a single-exponential rate constant of 0.065 $s^{-1}$. In contrast, $Tb^{3+}$ fluorescence produced by resonant energy transfer from MBP-C decreases in a single kinetic phase with a rate constant greater than 1 $s^{-1}$, implying that the slow change in tryptophan fluorescence monitors a conformational change that is not limited in rate by ion dissociation. The rate constants of the slow phases accompanying $Ca^{2+}$ binding and release are strongly affected by temperature and are weakly accelerated by the prolyl isomerase cyclophilin. These data strongly suggest that the binding of either $Ca^{2+}$ or $Tb^{3+}$ to MBP-C is coupled to a conformational change that involves the cis−trans isomerization of a peptide bond. Fitting of the data to kinetic models indicates that, in the absence of $Ca^{2+}$, the proline in approximately 80% of the molecules is in the trans conformation. The slow kinetics associated with cis−trans proline isomerization may be exploited by endocytic receptors to facilitate sorting of carbohydrate-bearing ligands from the receptor in the endosome.

The C-type animal lectins are a diverse family of proteins whose members contain a conserved $Ca^{2+}$-dependent carbohydrate-recognition domain (CRD[1]) (*1*). C-type lectins utilize carbohydrate binding for a wide range of purposes: mannose-binding proteins (MBPs), pulmonary surfactant proteins, and the macrophage mannose receptor bind to carbohydrate-rich pathogen cell surfaces as the first step of an antibody-independent immune response; selectins direct the trafficking of leukocytes to sites of inflammation and peripheral lymph nodes; and mammalian and avian hepatic lectins selectively remove serum glycoproteins by receptor-mediated endocytosis. The MBPs are well-characterized members of the C-type lectin family which are found in the serum and liver of mammals (*2*−*4*).

The three-dimensional structures of CRDs from seven different C-type lectins show that all possess a similar core structure. In addition, classical C-type lectins which bind carbohydrates share a $Ca^{2+}$-binding site (designated site 2 in the MBPs (*5*)) at which carbohydrates directly interact with the bound $Ca^{2+}$ as well as with amino acids that serve as $Ca^{2+}$ ligands (*6*−*9*). In the MBPs, which bind to two $Ca^{2+}$, this site is designated site 2 (*5*). The amino acid residues that comprise this binding site are highly conserved, especially a tripeptide sequence of two $Ca^{2+}$ ligands flanking a cis-proline residue (*10*). High-resolution crystal structures of several C-type lectins (*5*−*9*, *11*−*13*) show that the cis-proline positions the two flanking residues for interaction with $Ca^{2+}$, and it is not possible to position these two residues in a similar arrangement if the proline is in the trans configuration. Structural analysis of MBPs from rat liver (MBP-C) and serum (MBP-A) reveal that, when $Ca^{2+}$ is removed from site 2, the peptide bond preceding $Pro^{191}$ in

† This work is supported by grant GM50565 from the National Institutes of Health.

* To whom correspondence should be addressed at Department of Structural Biology, Fairchild Building, Stanford University School of Medicine, Stanford, CA 94305-5126. E-mail: weis@fucose.stanford.edu. Tel: (650) 725 4623. Fax: (650) 723 8464.

[1] Abbreviations: CDTA, cyclohexyldiaminetetracetic acid; EDTA, ethylenediaminetetraacetic acid; EGTA, ethyleneglycol bis(β-aminoethyl ether)- *N*,*N*,*N*′,*N*′-tetraacetic acid; DTT, dithiothreitol; $K_{app}$, apparent equilibrium dissociation constant; MBP, mannose-binding protein; PIPES, 1,4-piperazinediethanesulfonic acid; CRD, carbohydrate-recognition domain.

10.1021/bi9819733 CCC: $15.00 
Published on Web 12/01/1998

MBP-C (equivalent to $Pro^{186}$ in MBP-A) can adopt either the cis or trans conformation (*14*). The existence of alternate conformational states for this peptide bond in the absence of $Ca^{2+}$, and the apparently strict requirement for the cis conformation when $Ca^{2+}$ is bound, implies that the peptide conformation must change for a subset of $Ca^{2+}$-free molecules upon the binding of $Ca^{2+}$.

The isomerization of peptide bonds constitutes a slow, rate-limiting step in the folding of many proteins in vitro (*15*). Proline isomerization in peptides and proteins is a unimolecular process with a half-life of tens of seconds to several minutes at room temperature and physiological pH (*16*, *17*). Variations in rate likely depend on the coupling of the isomerization reaction to structural changes in adjacent parts of the protein. In addition to its well-demonstrated effects on protein folding, proline isomerization can account for slow conformational changes in folded proteins (*18*, *19*).

In this paper, the conformational changes associated with the binding of $Ca^{2+}$ to MBP-C are probed by measuring the effects of $Ca^{2+}$ on intrinsic tryptophan fluorescence. $Ca^{2+}$ binding or release involves a fast bimolecular step and a slow unimolecular step. Fluorescence resonant energy transfer from tryptophan to $Tb^{3+}$ indicates that the fast step corresponds to ion binding or release. The rate of the slow phase of fluorescence change is slightly accelerated by the addition of the prolyl isomerase cyclophilin, and this acceleration can be inhibited by cyclosporin A. The rate of the slow phase of the fluorescence change is also very sensitive to temperature. These data suggest that the slow step corresponds to the proline isomerization that has been observed in structures of $Ca^{2+}$-free MBPs (*14*). Modeling of the observed kinetics indicates that, in the absence of $Ca^{2+}$, the conserved proline in 80−85% of the molecules is in the trans conformation.

## EXPERIMENTAL PROCEDURES

*Materials*. Chelex-100 was obtained from Bio-Rad. $TbCl_3$ (99.99%) was obtained from Aldrich. EDTA, EGTA, and CDTA were obtained from Sigma. Cyclosporin A was obtained from Calbiochem. Spectra-Por 4 dialysis membrane was obtained from Spectrum and treated as described in ref *20* to remove metals and contaminants. All other chemicals were from J. T. Baker.

*Protein Purification*. Rat liver and serum MBPs were expressed in *Eschericia coli* as previously described (*21*). The proteins were purified using a procedure adapted from that used to purify recombinant chicken hepatic lectin (*22*). Cell paste from 5 L of *E. coli* was resuspended in 50 mL of buffer A (10 mM Tris-Cl pH 7.8, 3 mM $CaCl_2$) and stored at − 70 °C. Cells were thawed, the volume was brought to 200 mL with buffer A, and 0.2 mM PMSF was added. The extract was cooled on wet ice and subjected to 8 iterations of sonication (Branson sonicator) for 30 s followed by rest periods of 1 min. NaCl was added to a final concentration of 0.5 M, and the extract was centrifuged at 27000*g* for 30 min. The supernatant was passed through a 0.45 $\mu$m cellulose acetate syringe filter, and 200 mL of clarified extract was loaded onto a 30 mL mannose−Sepharose (*23*) column (10 × 3.5 cm) at a flow rate of 5 mL/minute. The pellet from the first centrifugation was resuspended in 80 mL buffer A, sonicated, brought to 0.5 M NaCl, clarified by centrifugation and filtration, and loaded onto the same mannose−Sepharose column used for the first extract. The affinity column was washed with 200 mL of loading buffer (25 mM Tris-Cl pH 7.8, 1.25 M NaCl, 2.5 mM $CaCl_2$), and the protein was selectively eluted from the mannose−Sepharose column with elution buffer (25 mM Tris-Cl pH 7.8, 1.25 M NaCl, 2.5 mM EDTA). The affinity-purified protein (approximately 10 mL x 0.15 mM) was adjusted to 12.5 mM $CaCl_2$, and the protein was equilibrated at 37 °C for 10 min. Elastase was added to a final concentration of 0.2 mg/mL, and the protein was digested for 2.5 h at 37 °C. PMSF (0.5 mM) and 0.05% Triton X-100 were then added to stop the digestion, and the sample was cooled on ice. This solution was loaded onto a 7 mL mannose−Sepharose column at a flow rate of approximately 0.5 mL/min. The column was washed with 5 mL of loading buffer containing 0.05% Triton X-100, followed by 10 mL of loading buffer without detergent, and then 20 mL of elution buffer. EDTA was added to the eluted protein (approximately 6 mL at 0.2 mM) to a final concentration of 2 mM to ensure metal ion removal. The solution was placed into a bag prepared from Spectra-por 4 membrane that had been washed at 80 °C for 6 h in four changes of Milli-Q (Millipore) treated water. The solution was dialyzed at 4 °C for 48 h against six changes of 0.8 L of reaction buffer (50 mM Tris-Cl pH 8.0 (measured at 22 °C), 100 mM NaCl) which had been scrubbed of metals by passing over a column of Chelex-100. The concentration of the dialyzed protein was estimated by measuring the absorbance at 280 nm in 6 M guanidine-HCl, 10 mM bis-Tris-Cl, pH 6.5, and calculating a molar extinction coefficient ($\epsilon$ = 14 420 $M^{-1}$ $cm^{-1}$) (*24*) for the fragment of MBP-C spanning residues 107−226 (numbering from mature N-terminus, mass 13367). This fragment is 2 residues longer than the previously described subtilisin fragment (*7*), and was identified on the basis of the mass determined by MALDI-TOF mass spectroscopy (mass 13 363) (Protein and Nucleic Acid Facility, Stanford University) and the observation of the C-terminal residue in several crystal structures (unpublished observations).

*Fluorescence Measurements*. Measurements were performed using an SLM 8000C fluorimeter with a 450 W lamp. Measurements were corrected for fluctuations in lamp intensity by dividing by the fluorescence of a rhodamine sample measured simultaneously. Emission spectra were recorded using excitation at 295 nm with an 8 nm band-pass and emission slits set for a 2 nm band-pass. Measurements were corrected for background and Raman scattering by subtracting the fluorescence measured from a sample of reaction buffer (50 mM Tris-Cl, pH 8.0, 100 mM NaCl or 25 mM Na−PIPES, pH 6.8, 100 mM NaCl; pH measured at 22 °C). By using published values for the variation of $pK_a$ as a function of temperature (*25*, *26*), we calculated the pH of these buffers to be 7.6 and 6.7 at 36 °C. Reactions with $Ca^{2+}$ were carried out at pH 7.6, whereas reactions with $Tb^{3+}$ were carried out at pH 6.7. The lower pH conditions in the reactions with $Tb^{3+}$ were necessary to avoid the formation of $Tb(OH)_3$ precipitates. Kinetic measurements of intrinsic tryptophan fluorescence were made using excitation light at 295 nm with 8 nm bandwidth and emission through a 340 nm band-pass filter with full-width at half-maximum of 4 nm. Tryptophan to $Tb^{3+}$ fluorescence resonant energy transfer was measured using excitation light at 295 nm with a 16 nm bandwidth, and emission through a long-pass filter

with 50% transmission at 510 nm. For time course studies, fluorescence intensity was integrated over 0.9 s and the step time was 1 s. Samples (2 mL) were magnetically stirred at low speed in a thermostated cuvette holder. Samples were diluted into degassed, prewarmed reaction buffer and allowed to equilibrate for 20 min prior to additions of $Ca^{2+}$ or $Tb^{3+}$. Additions of $Ca^{2+}$, $Tb^{3+}$, or chelator were made using 4−6 $\mu$L of concentrated solutions diluted in the reaction buffer. $CaCl_2$ and $TbCl_3$ stock solutions were normalized by titration against a standardized stock solution of EDTA (Fisher) by monitoring the end-point of titration with a pH meter (*27*). Stirring in the cuvette was turned to maximum immediately before and for 10 s following the addition of either metal ions or chelators. The half-time for mixing was measured to be less than one second in control experiments by observing the appearance of fluorescence upon addition of tryptophan to buffer.

Unless otherwise stated, the temperature of the sample in the fluorimeter was maintained at 36 °C using a water bath (Lauda). The temperature control was monitored using a thermocouple in control experiments and shown to vary by less than 0.2 °C over the course of an hour. The temperature in the cuvette was within 0.2 °C of the bath temperature, so no correction was made for the small difference in temperature between them. Temperature-dependent changes in pH, which are particularly large for Tris (*25*), were compensated for by adding small amounts of HCl to reaction buffers at lower temperatures. Control experiments showed that the moderate variation of pH as a function of temperature did not affect rates significantly even without adjusting the pH in this manner.

*Cyclophilin Catalysis*. *E. coli* cytoplasmic cyclophilin and human cyclophilin A were purified from *E. coli* expression systems as previously described (*28*, *29*); an additional purification step using cation exchange chromatography on either CM-cellulose or Mono S (Pharmacia) was added to improve protein purity, as assessed by SDS−PAGE. For the purification of the human enzyme, 1 mM dithiothreitol was added to buffer solutions during purification and storage. The enzymes were used within two weeks of purification and did not show significant changes in activity over that time. Cyclosporin A was dissolved in 50% ethanol/50% water at a concentration of 1 mM.

*Data Analysis*. The kinetics of fluorescence changes were fit to single-exponential curves using nonlinear least-squares regression according to the following equation:

$$F_t = F_\infty - [F_\infty - F_0]e^{-kt} \quad (1)$$

where $F_0$, $F_t$, and $F_\infty$ are the fluorescence at times 0, $t$ seconds, and roughly 8−10 half-lives following the start of the reaction. To control for small variations in pipetting of protein and in the placement of the cuvette in the fluorimeter, the fluorescence of each sample was normalized to the background-subtracted fluorescence of the initial $Ca^{2+}$-free sample, that is, before ions or chelators had been added. The fluorescence of different samples typically differed by less than 5%. Nonlinear least-squares regression was performed using the Marquardt algorithm as implemented in the programs KALEIDAGRAPH (Abelbeck Software) and DATAPLOT (NIST) (*30*). Kinetic simulations were performed using the programs KINSIM (*31*) and GEPASI (*32*). Parameters for kinetic models were fit using nonlinear least-squares methods implemented in the program FITSIM (*33*).

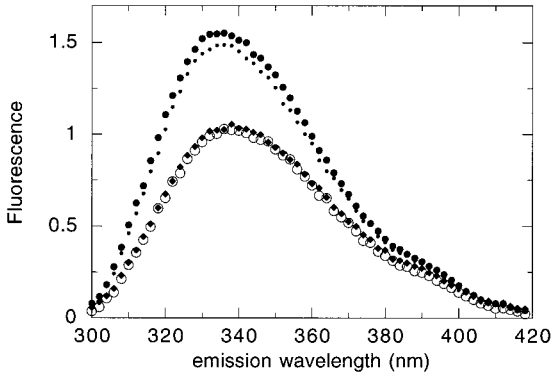


FIGURE 1: $Ca^{2+}$-induced change in intrinsic tryptophan fluorescence intensity. The addition of 0.2 mM $CaCl_2$ (small dots) and 0.4 mM $CaCl_2$ (large dots) to apo-MBP-C (open circles) causes a significant increase in fluorescence intensity and a small shift in the emission wavelength maximum. The addition of 1 mM EGTA returns the fluorescence to the level prior to the addition of $Ca^{2+}$ (diamonds). Spectra were recorded five minutes following the addition of $CaCl_2$ or EGTA. Conditions are the same as for all other experiments (1 $\mu$M apo-MBP-C, 40 mM Tris-Cl, pH 7.6, 150 mM NaCl) involving the addition of $CaCl_2$, except that the temperature was 32 °C.

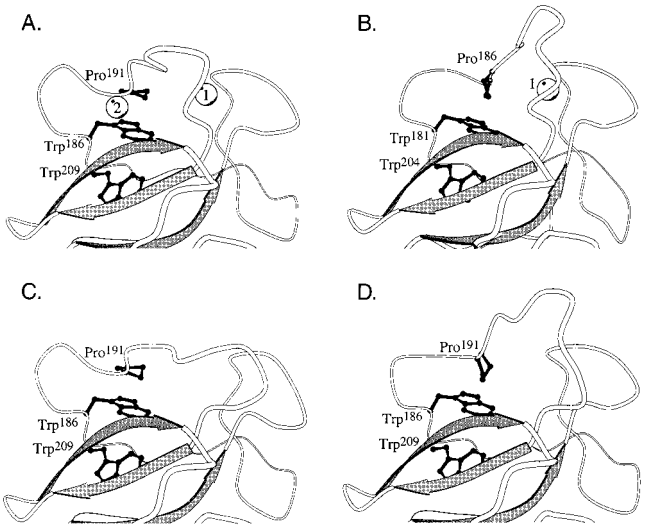


FIGURE 2: Proximity of tryptophan to $Ca^{2+}$-binding sites in MBP. Ribbon diagrams of the portion of the MBP CRD proximal to the two $Ca^{2+}$-binding sites (designated 1 and 2 in panel A). The conserved proline at $Ca^{2+}$ site 2 and the two conserved tryptophan residues in the hydrophobic core of the CRD are shown in black (A) 2-$Ca^{2+}$ MBP-C, (B) 1-$Ho^{3+}$ MBP-A, (C) apo-MBP-C copy 2 (cis-$Pro^{191}$), and (D) apo-MBP-C copy 1 (trans-$Pro^{191}$). The structure drawn in (A) was described in ref *7*, and the other structures are described in the preceding paper (*14*).

## RESULTS

*Equilibrium $Ca^{2+}$ Binding Monitored by Tryptophan Fluorescence*. Addition of $Ca^{2+}$ to apo-MBP-C produces an intensity increase and a small shift in the position of the emission wavelength maximum in the intrinsic tryptophan fluorescence spectrum of the protein (Figure 1). The change in fluorescence intensity likely reflects the proximity of the two tryptophan residues in the MBP-C CRD to the $Ca^{2+}$-binding sites (*5*) (Figure 2). $Ca^{2+}$-induced changes in tryptophan fluorescence have been reported for other C-type

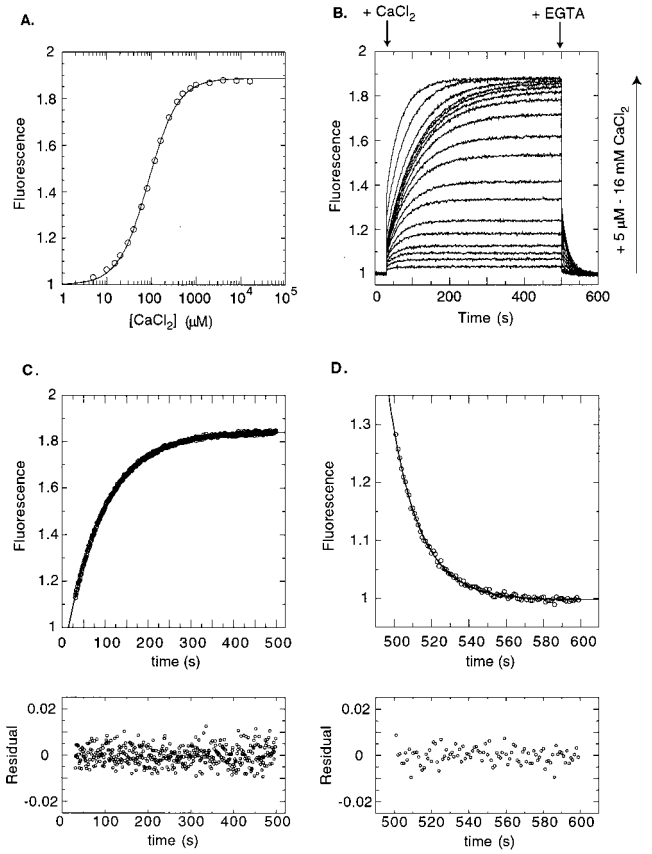


FIGURE 3: Equilibrium and kinetic measurements of $Ca^{2+}$-induced changes in tryptophan fluorescence. (A) The equilibrium level of fluorescence is plotted as a function of the concentration of $Ca^{2+}$. The data have been fitted to the equation $F = F_0 + (F_{max} - F_0)\text{-}([Ca^{2+}]^n/(K_{app} + [Ca^{2+}]^n))$, where $F_{max} = 1.89$, $K_{app} = 85\ \mu M$, and $n = 1.3$. (B) Progress curves of fluorescence changes as a function of $Ca^{2+}$. Apo-MBP-C (1 $\mu$M) in 40 mM Tris-Cl, pH 7.6, 150 mM NaCl was equilibrated at 36 °C for 15 min in the dark. Thirty seconds after starting the recording, stirring in the cuvette was increased to maximum and 4−16 $\mu$L of $CaCl_2$ solutions (2.5 mM − 2 M) was added, resulting in final concentrations of 5, 10, 15, 20, 30, 40, 60, 80, 120, 160, 250, 375, 500, 750, 1000, 2000, 4000, 8000, and 16 000 $\mu$M. Fluorescence measurements were resumed approximately 1 s following the addition of $CaCl_2$. Four-hundred and seventy seconds after the addition of $Ca^{2+}$, excess EGTA was added to a final concentration of 0.5 mM for $Ca^{2+}$ concentrations up to 250 $\mu$M, and to a final concentration of 20 mM for the higher concentrations of $Ca^{2+}$. The pH of each EGTA solution was adjusted to minimize the change in pH which results from the reaction of EGTA with $Ca^{2+}$. The slow phases following the addition of 1 mM $CaCl_2$ (C), or following the addition of 1.5 mM EGTA to protein equilibrated with 1 mM $CaCl_2$ (D), are fit to single exponentials (eq 1), and the residuals ($F_{obs} - F_{calc}$) are plotted.

lectins, including rat hepatic lectin (*34*), pulmonary surfactant protein A (*35*), and herring antifreeze protein (*36*). We have also observed $Ca^{2+}$-dependent changes in tryptophan fluorescence for MBP-A that are similar to those seen in MBP-C (not shown). The change in fluorescence upon $Ca^{2+}$ addition can be completely reversed by the addition of the divalent metal ion chelators EGTA (Figures 1 and 3), EDTA, and CDTA (not shown). The fluorescence intensity of apo- and $Ca^{2+}$-bound MBP-C, and in particular the change in fluorescence intensity upon adding $Ca^{2+}$, is very sensitive to changes in temperature. At 37 °C, the fluorescence intensity change is nearly 100% upon adding saturating amounts of $Ca^{2+}$, whereas the change is only about 20% at 20 °C. At all temperatures, the emission wavelength maximum undergoes a small blue shift from 337 to 334 nm upon $Ca^{2+}$ binding.

A binding curve relating tryptophan fluorescence to the concentration of free $Ca^{2+}$ gives an apparent equilibrium dissociation constant ($K_{app}$) of 85 $\mu$M and an apparent Hill coefficient of 1.3 (Figure 3A). The modest cooperativity seen in this binding curve is consistent with structural data indicating that the protein binds two $Ca^{2+}$ (*14*), as well as kinetic data presented below, and that the binding of $Ca^{2+}$ involves more than two states with distinct molar fluorescence values. The value of $K_{app}$ inferred from tryptophan fluorescence is lower than the previously published value of 1.2 mM obtained from the coupling of protease sensitivity and carbohydrate binding to $Ca^{2+}$ binding in MBP-A (*21*). Part of this discrepancy may be due to differences in the $Ca^{2+}$-binding sites of MBPs A and C. Although the geometry of the $Ca^{2+}$-binding sites in both proteins is very similar, two aspartic acid residues that serve as ligands in $Ca^{2+}$ site 1 in MBP-A are replaced by asparagine in MBP-C. The discrepancy between values of $K_{app}$ may also arise from differences in the way $Ca^{2+}$ binding couples to spectroscopic versus other indirect measures of $Ca^{2+}$ binding.

*Kinetics of $Ca^{2+}$ Binding Monitored by Tryptophan Fluorescence*. The kinetics of the $Ca^{2+}$-induced change in tryptophan fluorescence are biphasic over the range of $Ca^{2+}$ concentrations between 5 $\mu$M and 16 mM. A burst increase of fluorescence occurs within the dead time of mixing (approximately 1 s), which is followed by a much slower increase (Figure 3B). The amplitudes of both phases increase as the amount of added $Ca^{2+}$ is increased up to 1 mM. Above 1 mM, the burst-phase amplitude continues to increase, whereas the slow-phase amplitude decreases. The slow phase of the fluorescence increase fits very well to a single exponential (Figure 3C), but the rate constant of the exponential varies as a function of $Ca^{2+}$ concentration (Figure 4A). The rate constant shows a bell-shaped dependence upon $Ca^{2+}$ concentration, reaching a minimum value at 1 mM $Ca^{2+}$ of 0.01 $s^{-1}$, and maximum values of 0.045 and 0.036 $s^{-1}$ at the lowest and highest concentrations of $Ca^{2+}$ tested. In a separate series of experiments at higher concentrations of $Ca^{2+}$, the rate constant of the slow phase plateaus at roughly 0.04 $s^{-1}$ (not shown).

$Ca^{2+}$-dependent changes in tryptophan fluorescence were measured over a wide range of protein concentrations to test if inner filter effects or bimolecular binding events such as aggregation affect the observed kinetics. The fluorescence of apo-MBP and $Ca^{2+}$-saturated MBP is linearly dependent on protein concentration over the range of 89 nM to 2.9 $\mu$M (Figure 5A), indicating that such effects are not significant over this range of protein concentration. Furthermore, progress curves measured after adding saturating $Ca^{2+}$ to apo-MBP over this range of protein concentration are superimposable if they are scaled relative to the amount of protein present in the sample (not shown). Finally, fitting the slow phase to a single exponential shows that the rate constant varies by less than 10% with protein concentration (Figure 5B). Thus, the slow phase of tryptophan fluorescence change shows first-order kinetics with respect to protein concentration, and the variation in the rate constant of the slow phase as a function of $Ca^{2+}$ concentration is not due to a rate-limiting bimolecular binding event.

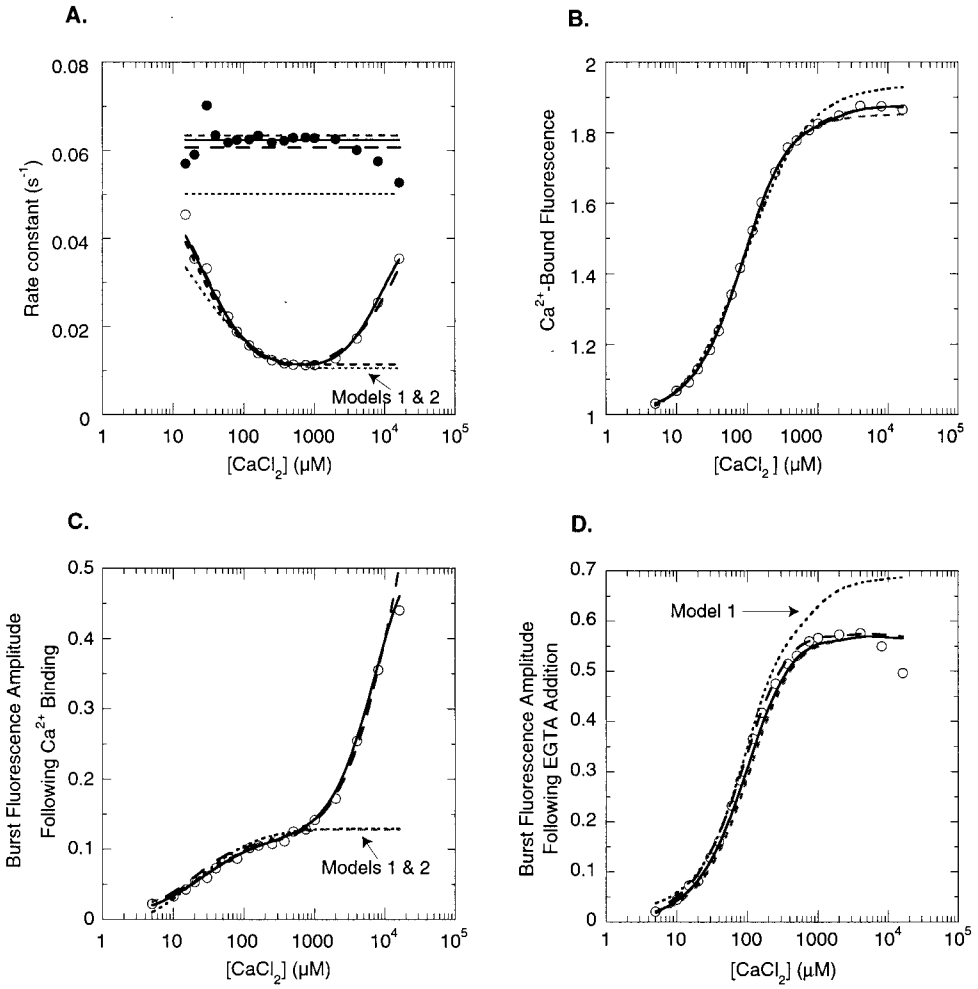


FIGURE 4: Rates and amplitudes of kinetic phases, compared with predictions from four kinetic models. Experimental observations are derived from the experiment described in Figure 3. (A) The variation in the rate constants of the slow phase following the addition of $Ca^{2+}$ (open circles) and following the subsequent addition of excess EGTA (solid circles) is compared to the variation in rate constants predicted by the kinetic models shown in Figure 6: model 1, fine dashed line; model 2, medium-fine dashed line; model 3; coarse dashed line; model 4, solid line. (B) Comparison of the final equilibrium fluorescence value with the kinetic models. (C) Comparison of amplitudes for the burst phase increase following the addition of $CaCl_2$ with models. (D) Comparisons of the burst-phase amplitude decrease following the addition of EGTA with models.

In parallel studies on a form of MBP-A containing the CRD and the adjacent trimerization domain, $Ca^{2+}$-dependent changes in fluorescence intensity show a more complex behavior where the amplitudes and rate constants of fluorescence changes are very sensitive to protein concentration (not shown). The mechanism responsible for the difference in behavior of the MBP-A CRD plus trimerization domain compared to the data from the MBP-C CRD shown here is unclear. The effect may be due in part to aggregation, since, unlike MBP-C (Figure 5A), a plot of fluorescence versus protein concentration for apo-MBP-A shows a downward inflection over the range 50 nM to 1 $\mu$M protein (not shown).

*Mechanism of $Ca^{2+}$ Binding.* The structural observations reported in the previous paper (*14*) suggest that the burst phase of fluorescence may be due to $Ca^{2+}$ binding by the fraction of molecules in which proline at site 2 adopts the cis conformation, and that the slow step is due to the isomerization of the peptide bond preceding $Pro^{191}$ in those molecules containing a trans proline in the absence of $Ca^{2+}$. Prolyl peptide bond isomerization is a slow unimolecular process with rate constants in the range of $0.1-0.01$ $s^{-1}$ at 36 °C (*17*). The effect of $Ca^{2+}$ concentration on the slow rate of change in tryptophan fluorescence (Figure 4A) suggests a multistep mechanism that relates changes in tryptophan fluorescence to $Ca^{2+}$ binding, with a fast phase due to rapid ion binding and a slower phase due to conformational changes. The two most interesting features of these data are the decrease of the rate constant of the slow phase as the concentration of added $Ca^{2+}$ increases up to 1 mM, and the increase of the rate constant of the slow phase as the concentration of added $Ca^{2+}$ increases above 1 mM.

Several kinetic models involving isomerization steps coupled to ion-binding steps were tested for their ability to model the changes in fluorescence as a function of $Ca^{2+}$ concentration. Of these, only the simplest models which successfully predict key features of the observed data are presented here (Figure 6). For each model, rate constants and molecular fluorescence values, as well as the residuals between predicted and observed progress curves, were optimized by nonlinear least-squares minimization using the programs KINSIM (*31*) and FITSIM (*33*) (Figures 6 and 7, and Table 1). The two simplest schemes (models 1 and 2, Figure 6A,B) were used to model progress curves measured in the presence of 5 $\mu$M to 1 mM $Ca^{2+}$, whereas two more

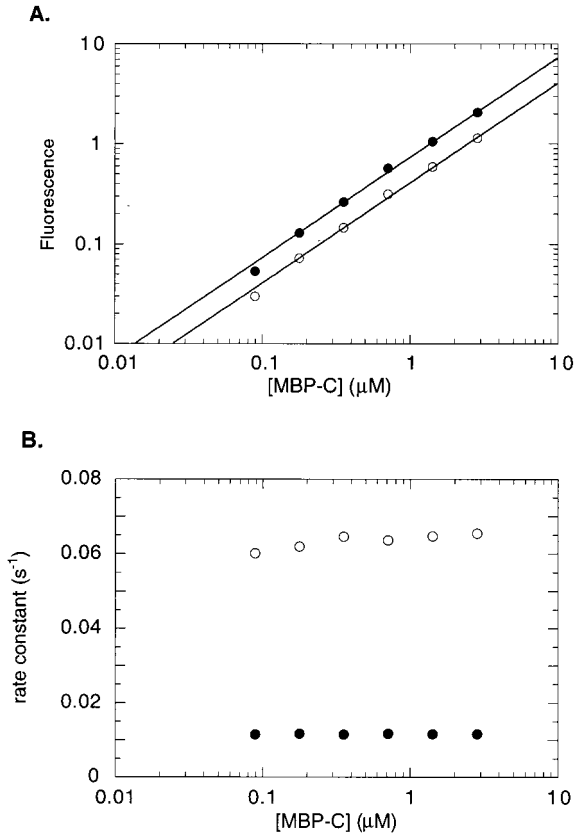


FIGURE 5: Effects of protein concentration on fluorescence changes. (A) The fluorescence of apo-MBP-C (open circles) and MBP-C plus 1 mM $CaCl_2$ (solid circles) was measured in 40 mM Tris-Cl, pH 7.6, 150 mM NaCl at 36 °C. The protein was allowed to equilibrate for 15 min following dilution and 8 min following the addition of $CaCl_2$. (B) The rates of the slow phase following the addition of 1 mM $CaCl_2$ (solid circles) to apo-MBP-C and the slow phase following the addition of 2 mM EDTA (open circles) to MBP-C equilibrated with 1 mM $CaCl_2$ were fit to a single-exponential decay (eq 1), and the rate constants are plotted against the concentration of protein.

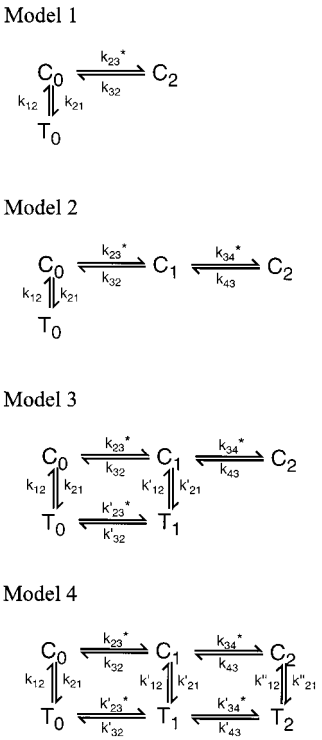


FIGURE 6: Kinetic models. States $T_x$ and $C_x$ represent forms of MBP-C with the peptide preceding $Pro^{191}$ in the trans and cis conformations respectively, and where $x$ denotes the number of $Ca^{2+}$ bound to the protein. Unimolecular isomerization rate constants: $k_{12}$, $k_{21}$, $k'_{12}$, $k'_{21}$, $k''_{12}$, and $k''_{21}$. Pseudo-first-order rate constants ($k[Ca^{2+}]$, where $k = 10^6$ $M^{-1}$ $s^{-1}$): $k_{23}$*, $k_{34}$*, $k'_{23}$*, and $k'_{34}$*. Unimolecular $Ca^{2+}$ dissociation rate constants: $k_{32}$, $k_{43}$, $k'_{32}$, and $k'_{43}$.

complex schemes (models 3 and 4, Figure 6C,D) were used to model progress curves measured in the presence of 5 $\mu$M to 16 mM $Ca^{2+}$. In addition, the parameter fitting for each model included data from an additional progress curve that was recorded after adding excess EGTA to $Ca^{2+}$-saturated protein.

A simple three-state model consisting of a slow, reversible unimolecular isomerization followed by a $Ca^{2+}$-binding step with a first-order dependence on $Ca^{2+}$ concentration (model 1, Figure 6A) qualitatively models the decrease in rate constant as the concentration of $Ca^{2+}$ is increased from 5 $\mu$M to 1 mM. Analytical expressions can be derived for the time-dependent concentrations of all species in this model, given initial conditions and rate constants (*37*, *38*). In the experiments reported here, the bimolecular step involving $Ca^{2+}$ binding is pseudo-first-order (denoted as $k_{23}$* in Figure 6A; all pseudo-first-order steps involving bimolecular $Ca^{2+}$-binding steps are denoted by asterisks in this paper), because the amount of $Ca^{2+}$ present is in excess over the amount of protein, and the concentration of $Ca^{2+}$ is effectively constant during the measurement of the progress curve. Thus, for the three-state case, the time-dependent concentration of each species can be described as the sum of two exponentials with time constants $\tau$ that are related to the kinetic rate constants by the following relationships (*38*):

$$\tau_1^{-1} = [M + (M^2 - 4N)^{1/2}]/2 \quad (2a)$$

$$\tau_2^{-1} = [M - (M^2 - 4N)^{1/2}]/2 \quad (2b)$$

where

$$M = k_{12} + k_{21} + k_{23}^* + k_{32}$$
$$N = k_{12}(k_{23}^* + k_{32}) + k_{21}k_{32}$$

Under the conditions of the experiment, $\tau_1^{-1} \gg \tau_2^{-1}$ and $k_{23}$*, $k_{32} \gg k_{12}$, $k_{21}$, leading to the following simplified forms (*39*)

$$\tau_1^{-1} = k_{23}^* + k_{32} \quad (3a)$$

$$\tau_2^{-1} = k_{12} + k_{21}/(1 + k_{23}^*/k_{32}) \quad (3b)$$

Because all measurements were made on a time scale of seconds, $\tau_1$ is not precisely defined by the current set of experiments. However, a lower bound of 1 $s^{-1}$ can be set for $k_{23}$*, as only a single slow exponential phase is seen following the initial burst phase. If $k_{23}^* = k[Ca^{2+}]$ (Figure 6A), where $k$ is the bimolecular rate constant, then $k \geq 10^5$ $M^{-1}$ $s^{-1}$. Values of $k < 10^5$ $M^{-1}$ $s^{-1}$ produce progress curves in which the rate constant of the burst phase at low concentrations of $Ca^{2+}$ is slower than that observed by manual mixing. This lower limit on the bimolecular rate constant is reasonable in light of studies on the binding of $Ca^{2+}$ to small molecule chelators and EF-hand $Ca^{2+}$-binding

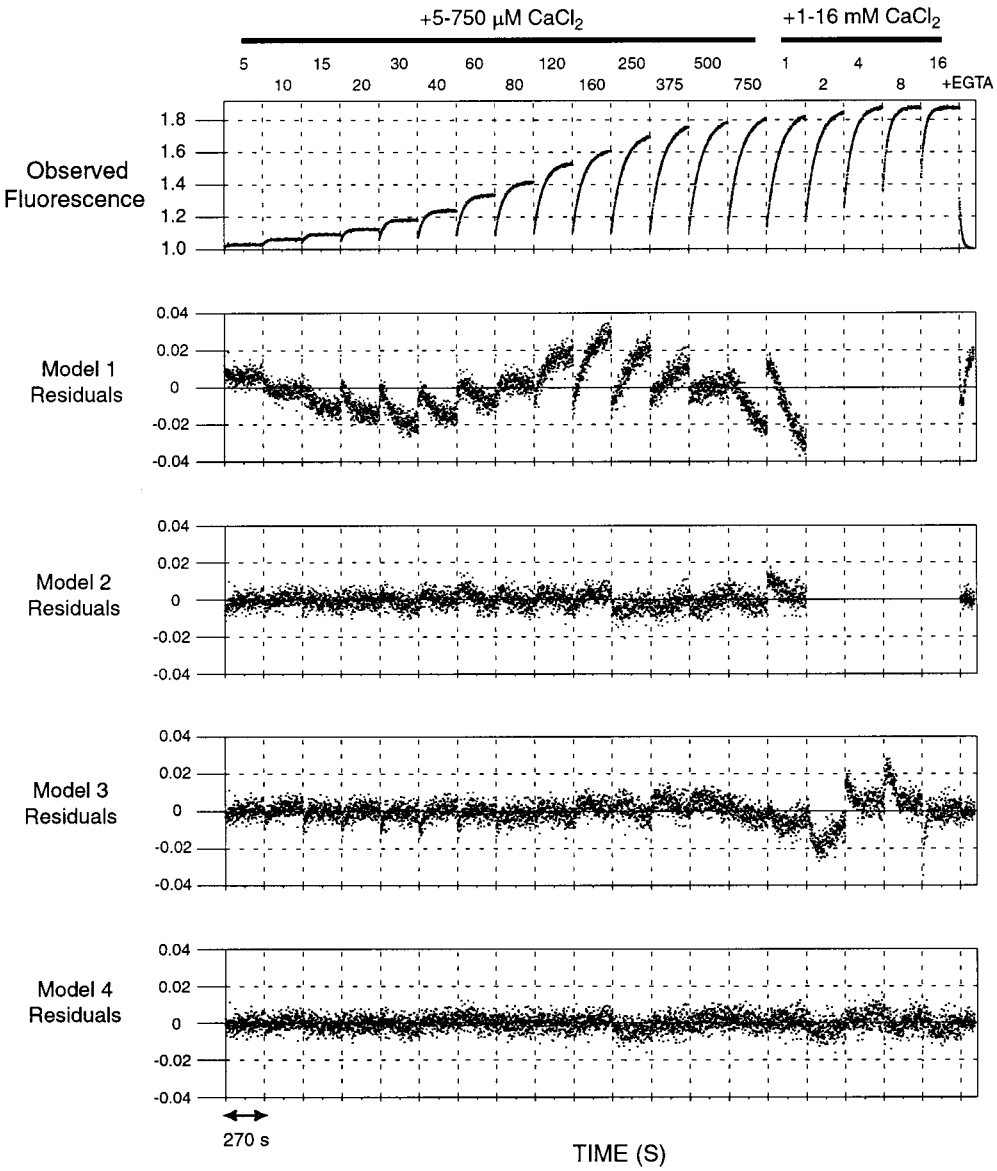


FIGURE 7: Residuals ($F_{obs} - F_{calc}$) between observed progress curves and progress curves predicted by kinetic models. The 20 progress curves shown in Figure 3B were fit to four different kinetic models (Figure 6) using FITSIM. The amount of $CaCl_2$ added prior to the recording of each curve is denoted above each progress curve at the top of the figure. Only the first 270 s of the progress curves following the addition of $CaCl_2$ to apo-MBP-C were included in the fitting to avoid overweighting the final equilibrium fluorescence values. Each box along the horizontal axis shows the first 270 s of the progress curve (top panel) measured at the $Ca^{2+}$ concentration shown at the top. Residuals for the four kinetic models shown in Figure 6 are shown in the lower panels, plotted underneath the corresponding progress curve. Models 1 and 2 (Figure 6A,B) are fitted only to the first 15 curves, and the curve produced after the addition of 1.5 mM EGTA to protein equilibrated with 1 mM $CaCl_2$, because these models cannot fit the increase in rates seen at higher concentrations of $CaCl_2$ (see Figure 4A). Models 3 and 4 (Figure 6C,D) are fitted to all 19 curves, as well as the curve produced after the addition of EGTA to the $Ca^{2+}$-bound protein.

proteins, where rate constants are typically $10^8-10^9$ $M^{-1}$ $s^{-1}$ for chelators (*40*, *41*) and $10^6-10^8$ $M^{-1}$ $s^{-1}$ for EF-hand proteins (*42*). According to eq 3b, the $Ca^{2+}$ concentration dependence of the rate of the slow phase is sensitive only to the ratio of $k_{23}*/k_{32}$ so long as $k \geq 10^5$ $M^{-1}$ $s^{-1}$. In this study, the bimolecular rate constant $k$ has been set to $10^6$ $M^{-1}$ $s^{-1}$ during parameter optimization using FITSIM, but the real value may be up to 10-fold lower or 100-fold higher. Likewise, the values of the other pseudo-first-order rate constants ($k_{34}*$, $k'_{23}*$, and $k'_{34}*$) in the four models in Figure 6 were calculated by assuming that the bimolecular rate constant $k$ was $10^6$ $M^{-1}$ $s^{-1}$. Because the experiments reported here only define the ratios of $k_{23}*/k_{32}$, $k_{34}*/k_{43}$, $k'_{23}*/k'_{32}$, and $k'_{34}*/k'_{43}$, it is important to note that the absolute values of the dissociation rate constants for all $Ca^{2+}$-release steps ($k_{32}$, $k_{43}$, $k'_{32}$, and $k'_{43}$) may also be up to 10-fold lower or 100-fold higher than the values reported in Table 1. The ratios of pairs of association and dissociation rate constants for each equilibrium have much lower errors, but the values of the errors are difficult to estimate. The errors on the parameters reported in Table 1 are lower estimates from the linear approximation of the error in the nonlinear regression algorithm.

Optimizing the parameters of model 1 (Figure 6A) using FITSIM shows that this simple mechanism accounts for the decrease in the rate of the slow phase as the concentration of $Ca^{2+}$ increases (Figure 4A). However, a closer examination of the residuals from progress curves predicted by model

Table 1. Refined Kinetic Parameters[a]

| | rate ($s^{-1}$) | | molar fluorescence ($10^6 \times M^{-1}$) | | initial concentration ($\mu$M) |
|---|---|---|---|---|---|
| | A. Three-State Model (Model 1)[b] | | | | |
| $k_{12}$ | $0.0098 \pm 0.00005$ | $T_0$ | $0.905 \pm 0.0008$ | $T_0$ | 0.80 |
| $k_{21}$ | $0.0404 \pm 0.0003$ | $C_0$ | $1.29 \pm 0.002$ | $C_0$ | 0.20 |
| $k_{23}$* | ($10^6$ $M^{-1}$ $s^{-1}$) | $C_2$ | $2.00 \pm 0.002$ | | |
| $k_{32}$ | $20.9 \pm 1.5$ | | | | |
| | B. Four-State Model (Model 2)[c] | | | | |
| $k_{12}$ | $0.0113 \pm 0.00002$ | $T_0$ | $0.933 \pm 0.0003$ | $T_0$ | 0.80 |
| $k_{21}$ | $0.0521 \pm 0.0002$ | $C_0$ | $1.31 \pm 0.0008$ | $C_0$ | 0.20 |
| $k_{23}$* | ($10^6$ $M^{-1}$ $s^{-1}$) | $C_1$ | $1.68 \pm 0.004$ | | |
| $k_{32}$ | $18.9 \pm 0.1$ | $C_2$ | $1.89 \pm 0.0006$ | | |
| $k_{34}$* | ($10^6$ $M^{-1}$ $s^{-1}$) | | | | |
| $k_{43}$ | $124 \pm 1$ | | | | |
| | C. Five-State Model (Model 3)[d] | | | | |
| $k_{12}$ | $0.0089 \pm 0.00003$ | $T_0$ | $0.947 \pm 0.0004$ | $T_0$ | 0.85 |
| $k_{21}$ | $0.0518 \pm 0.0003$ | $T_1$ | $2.13 \pm 0.01$ | $C_0$ | 0.15 |
| $k'_{12}$ | $0.0070 \pm 0.0001$ | $C_0$ | $1.30 \pm 0.001$ | | |
| $k'_{21}$ | $0.0041 \pm 0.0001$ | $C_1$ | $2.12 \pm 0.008$ | | |
| $k_{23}$* | ($10^6$ $M^{-1}$ $s^{-1}$) | $C_2$ | $1.87 \pm 0.0004$ | | |
| $k_{32}$ | $25.4 \pm 0.2$ | | | | |
| $k_{34}$* | ($10^6$ $M^{-1}$ $s^{-1}$) | | | | |
| $k_{43}$ | $91.7 \pm 2.0$ | | | | |
| $k'_{23}$* | ($10^6$ $M^{-1}$ $s^{-1}$) | | | | |
| $k'_{32}$ | $23900 \pm 500$ | | | | |
| | D. Six-State Model (Model 4)[e] | | | | |
| $k_{12}$ | $0.0109 \pm 0.00004$ | $T_0$ | $0.934 \pm 0.0003$ | $T_0$ | 0.82 |
| $k_{21}$ | $0.0515 \pm 0.0002$ | $T_1$ | $1.10 \pm 0.01$ | $C_0$ | 0.18 |
| $k'_{12}$ | $0.0067 \pm 0.0002$ | $T_2$ | $1.51 \pm 0.008$ | | |
| $k'_{21}$ | $0.00026 \pm 0.00008$ | $C_0$ | $1.31 \pm 0.001$ | | |
| $k''_{12}$ | $0.049 \pm 0.0006$ | $C_1$ | $1.83 \pm 0.005$ | | |
| $k''_{21}$ | $0.000 \pm 0.000$ | $C_2$ | $1.87 \pm 0.0006$ | | |
| $k_{23}$* | ($10^6$ $M^{-1}$ $s^{-1}$) | | | | |
| $k_{32}$ | $22.1 \pm 0.1$ | | | | |
| $k_{34}$* | ($10^6$ $M^{-1}$ $s^{-1}$) | | | | |
| $k_{43}$ | $140 \pm 3$ | | | | |
| $k'_{23}$* | ($10^6$ $M^{-1}$ $s^{-1}$) | | | | |
| $k'_{32}$ | $5790 \pm 390$ | | | | |
| $k'_{34}$* | ($10^6$ $M^{-1}$ $s^{-1}$) | | | | |
| $k'_{43}$ | $6110 \pm 280$ | | | | |

[a] Rate constants marked with asterisks denote pseudo-first-order rate constants set to $10^6$ $M^{-1}$ $s^{-1}$ [$Ca^{2+}$]. The three- and four-state models were fitted to progress curves measured following the addition of 5, 10, 15, 20, 30, 40, 60, 80, 120, 160, 250, 375, 500, 750, and 1000 $\mu$M $CaCl_2$, as well as the curve measured following the addition of 1.5 mM EGTA to the protein equilibrated with 1 mM $CaCl_2$. The five- and six-state models were fit to these sixteen progress curves, as well as curves measured following the addition of 2, 4, 8, and 16 mM $CaCl_2$. Refined parameters, standard errors, and the sum of square residual were computed using the program FITSIM (*33*). [b] Sum of squared residuals 0.620, 4165 data points, and 8 free parameters. [c] Sum of squared residuals 0.077, 4165 data points, and 10 free parameters. [d] Sum of squared residuals 0.206, 5249 data points, and 14 free parameters. [e] Sum of squared residuals 0.084, 5249 data points, and 18 free parameters.

1 reveals systematic deviations (Figure 7) which suggest that it is only a crude model of the physical system. Changing the order of the binding step relative to the isomerization, or giving the $Ca^{2+}$-binding step a second-order dependence on $Ca^{2+}$ concentration (i.e., $k_{23}^* = k[Ca^{2+}]^2$), both worsen the fit of the model (not shown). An alternative explanation for the poor fit of model 1 to the data might be the presence of additional intermediate states. A physically reasonable intermediate state which is not found in model 1 is a 1-$Ca^{2+}$ intermediate bridging the 0 and 2-$Ca^{2+}$ states. Inclusion of this intermediate leads to a four-state model (model 2, Figure 6B) that better fits the observed kinetics (Figure 7). This model introduces two additional parameters, and refining the parameters using FITSIM leads to a model which quantitatively accounts for all of the kinetics observed at physiologically relevant levels of $Ca^{2+}$ below 1 mM.

The increase in rate constant at concentrations of $Ca^{2+}$ that are higher than physiological levels can be modeled by more complex five-state and six-state models (models 3 and 4, Figure 6C−D, Figure 7). These models invoke physically reasonable intermediates, but contain too many parameters to be uniquely defined by the experiments reported in this study.

In each model shown in Figure 6 and Table 1, the ratio of $k_{12}$ and $k_{21}$ indicates that, in the absence of $Ca^{2+}$, 80−85% of the molecules contain the conserved proline at site 2 in the trans conformation. This ratio is similar to that seen in small peptides in aqueous solution (*16*).

*Dissociation of $Ca^{2+}$ from MBP-C Following the Addition of $Ca^{2+}$ Chelators*. The addition of $Ca^{2+}$ chelators with fast binding kinetics causes a reduction in the concentration of free $Ca^{2+}$ to subnanomolar levels within fractions of a second (*40*). When $Ca^{2+}$ chelators are added to $Ca^{2+}$-containing samples of MBP-C, the tryptophan fluorescence decreases to the original level before exposure to $Ca^{2+}$ (Figures 1 and 3B). The kinetics of this fluorescence decrease is biphasic, like the kinetics of the $Ca^{2+}$-induced fluorescence increase. A burst phase occurs faster than the dead time of mixing, which is followed by a slow phase that fits a single exponential (Figure 3D). Unlike the slow phase following the addition of $Ca^{2+}$, the rate of the slow phase following chelator addition does not vary significantly over the range of $Ca^{2+}$ concentration from 5 $\mu$M to 16 mM (Figure 4A). The amplitudes of both slow phases increase in a sigmoidal fashion as the amount of $Ca^{2+}$ added to the protein (prior to the addition of the $Ca^{2+}$ chelator) is increased (Figure 4C−D). Relatively small variations in the rate constants are seen at the extremes of $Ca^{2+}$ concentrations, which can be attributed in part to two distinct experimental limitations. At low concentrations of $Ca^{2+}$, the determination of the rate constant is less accurate because of the small amplitude of the fluorescence change. At high concentrations of $Ca^{2+}$, the determination of the rate constant is less accurate because the reaction of EGTA with $Ca^{2+}$ releases millimolar amounts of protons which overwhelm the capacity of the buffer and induce secondary effects on the rate of reaction between chelator and metal, as well as on the fluorescence of the protein itself. Nevertheless, at least over the range of 0.01−4 mM $Ca^{2+}$, the rate constant does not vary more than 10%.

As in the case of the $Ca^{2+}$-binding phases, the rate constant of the slow monoexponential decrease in fluorescence following the addition of chelator does not vary significantly as a function of protein concentration over the range from 0.09 to 2.9 $\mu$M (Figure 5B). The rate of the slow phase following the addition of chelator to $Ca^{2+}$-bound protein is first-order with respect to protein concentration, which supports the interpretation that the slow phase is associated with a unimolecular conformational change in the protein.

*Demonstration of Fast Ion Dissociation Followed by Slow Protein Conformational Change using Fluorescence Resonant Energy Transfer to $Tb^{3+}$*. Biochemical and structural studies indicate that lanthanides mimic the binding of $Ca^{2+}$ to MBP-A (*5*, *21*, *43*). Replacement of $Ca^{2+}$ with $Tb^{3+}$ is

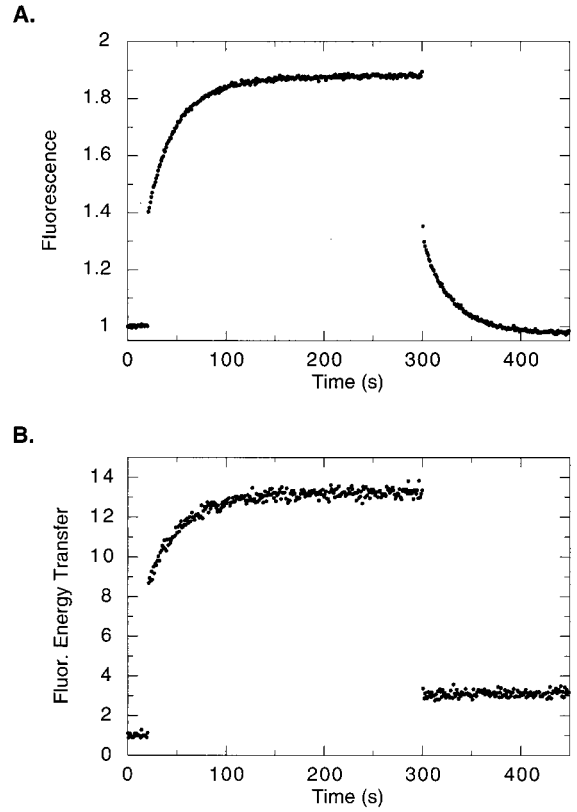


FIGURE 8: Effects of $Tb^{3+}$ binding on intrinsic tryptophan fluorescence and fluorescence energy transfer. At 20 s following the start of recording, 2 $\mu$M $TbCl_3$ was added to 0.36 $\mu$M apo-MBP-C in 25 mM NaPIPES, pH 6.7, 100 mM NaCl, 36 °C. Two-hundred and eighty seconds later, 2 mM EDTA was added. (A) Intrinsic tryptophan fluorescence was measured using a 340 nm band-pass filter. (B) Fluorescence resonant energy transfer from tryptophan to $Tb^{3+}$ was measured using a 510 nm high-pass filter. The level of fluorescence detected above 510 nm does not return to the original level following the addition of EDTA because the $Tb^{3+}$−EDTA complex fluoresces weakly. The difference between the level of fluorescence after adding chelator and the level before adding $Tb^{3+}$ is the same as the level of fluorescence from the same amount of $Tb^{3+}$ added to the buffer plus chelator in the absence of protein (not shown).

advantageous because the intrinsic fluorescence of $Tb^{3+}$ can be excited through nonradiative resonant energy transfer from tryptophan residues near the bound $Tb^{3+}$ (*44*). In this process, light at 295 nm is absorbed by tryptophan in MBP and energy is transferred to $Tb^{3+}$, leading to the emission of light at 545 nm. Accompanying this process is the less efficient direct excitation of fluorescence from free $Tb^{3+}$. Monitoring $Tb^{3+}$ fluorescence at 545 nm therefore corresponds to direct observation of ion binding and dissociation, independent of protein conformational changes.

The addition of nanomolar amounts of $Tb^{3+}$ to apo-MBP-C induces changes in tryptophan fluorescence that are similar to those induced by micromolar amounts of $Ca^{2+}$ (Figure 8), indicating that $Tb^{3+}$ can substitute for $Ca^{2+}$ in this protein. A binding curve similar to that performed with $Ca^{2+}$ could not be performed under conditions where the amount of $Tb^{3+}$ was in excess of the amount of protein, because of the tight binding. At the lowest level of protein (20 nM) yielding reasonable titration curves, the apparent dissociation constant is roughly 30 nM at pH 6.7, 36 °C. Under these conditions, the amount of free $Tb^{3+}$ is significantly reduced from the amount added, indicating an upper limit for $K_{app}$ of roughly 20 nM. These observations differ from measurements of $K_{app}$ for the binding of $Ho^{3+}$ to MBP-A. Limited proteolysis and carbohydrate binding coupled to $Ho^{3+}$ binding yield values for $K_{app}$ of 36 and 43 $\mu$M, respectively (*21*). As discussed above for $Ca^{2+}$, these higher values may reflect the replacement of two aspartic acid residues with asparagine in $Ca^{2+}$ site 1 of MBP-C, or differences in the behavior of $Ho^{3+}$ versus $Tb^{3+}$. The previous experiments may also have given higher estimates of $K_{app}$ because of the higher protein concentration used (25 $\mu$M with MBP-A versus 20 nM with MBP-C) or differences in buffer conditions (50 mM Tris-Cl pH 7.8 with MBP-A versus 25 mM Na-PIPES pH 6.7 with MBP-C).

A plot of energy transfer as a function of $Tb^{3+}$ concentration (not shown) produces a slightly different binding curve compared to that determined by tryptophan fluorescence, but the tight binding and the weaker energy transfer signal compared to tryptophan fluorescence prevent the determination of an accurate $K_{app}$. The binding of $Tb^{3+}$ to MBP-C results in a net increase in tryptophan fluorescence even in the presence of energy transfer, presumably because the energy transfer is weak and does not significantly reduce the gain in quantum yield due to the $Tb^{3+}$-induced change in the environment of the tryptophan residues (Figure 2).

The kinetics of $Tb^{3+}$-induced changes in tryptophan fluorescence and energy transfer is similar to the kinetics of $Ca^{2+}$-induced changes in tryptophan fluorescence, with one important exception. For both tryptophan fluorescence and energy transfer, the addition of $Tb^{3+}$ to the apoprotein gives rise to a burst phase and a slow phase (Figure 8A), the latter of which can be fit to a single exponential. For tryptophan fluorescence, the addition of a $Tb^{3+}$ chelator (such as EGTA, EDTA, or CDTA) causes a biphasic decrease in fluorescence, where the rate of the slow phase is identical to that seen upon adding chelators to $Ca^{2+}$-saturated protein. However, the change in energy transfer upon adding chelator is fast and monophasic (Figure 8B).

The clear difference between tryptophan fluorescence and energy transfer upon the addition of chelator suggests that the burst phase is associated with a fast ion dissociation process, whereas the slow phase is a protein conformational change not limited in rate by ion dissociation. This interpretation is consistent with the observation that the rate and amplitude of the slow phase are independent of the identity of the ion bound to the protein or of the kind or concentration of the chelator, so long as the chelator is added in excess. These observations are also consistent with kinetic schemes that include a slow, unimolecular prolyl peptide-bond isomerization step preceding one or more fast $Ca^{2+}$-binding steps (Figure 6).

*Temperature Dependence of Tryptophan Fluorescence Changes*. Because the rate of prolyl peptide-bond isomerization is known to be very sensitive to temperature, the rate of the $Ca^{2+}$-dependent change in tryptophan fluorescence was measured as a function of temperature. The rates of the slow phase of tryptophan fluorescence changes upon $Ca^{2+}$ binding or chelator addition show a strong temperature dependence (Figure 9). Arrhenius plots over the range of temperature from 21 to 42 °C are linear and the slopes correspond to activation enthalpies of 26 kcal/mol for the fluorescence increase coupled to $Ca^{2+}$ binding and 39 kcal/mol for the fluorescence decrease coupled to chelator addition.

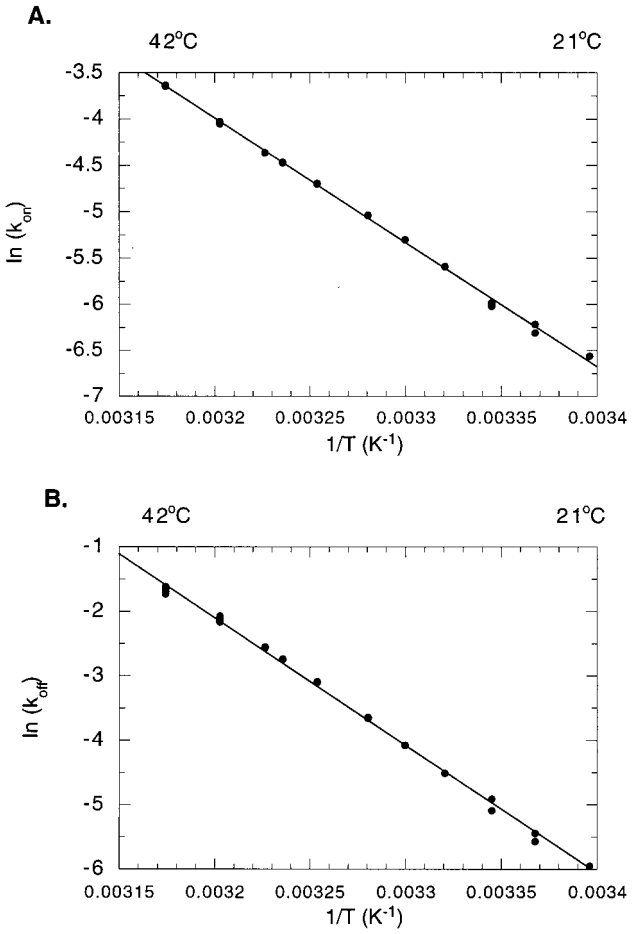


FIGURE 9: Arrhenius plots. The natural logarithm of the rate constant of the slow phase following the addition of 0.5 mM $CaCl_2$ to 0.5 $\mu$M apo-MBP-C (A) and the subsequent addition of 1 mM EGTA to the protein equilibrated with $Ca^{2+}$ (B) is plotted against the reciprocal of the absolute temperature. The data are fitted to the equation $\ln k = \ln A - E_a/RT$. The slopes give $E_a = 26.7$ and 39.4 kcal/mol, which correspond to $\Delta H^{\ddagger} = 26.1$ and 38.8 kcal/mol, calculated according to ref *38*.

According to the kinetic schemes described previously (Figure 6), the rate constant for the slow phase following the binding of $Ca^{2+}$ reflects the single microscopic rate constant for the conversion of apo-MBP-C containing trans-$Pro^{191}$ to the form of the protein containing cis-$Pro^{191}$, because the bimolecular $Ca^{2+}$-binding steps are much faster than the unimolecular conformational change (eq 3a). In contrast, the rate constant for the slow phase of the fluorescence change following the addition of EGTA is the sum of two microscopic rate constants for the interconversion of cis and trans forms of $Pro^{191}$ (eq 3b). The activation enthalpies for the slow reactions are higher than those reported for proline isomerization reactions in small peptides and denatured proteins, which are typically about 20 kcal/mol (*17*). Experimental errors such as inaccurate temperature control or changes in pH due to temperature have been carefully controlled and cannot account for these relatively large values. The high activation enthalpies associated with the slow tryptophan fluorescence changes in MBP-C are consistent with computational (*45*) and experimental (*46*) studies which suggest that steric restrictions on either ground-state or transition-state prolyl peptide conformations can have large effects on activation enthalpies and kinetics.

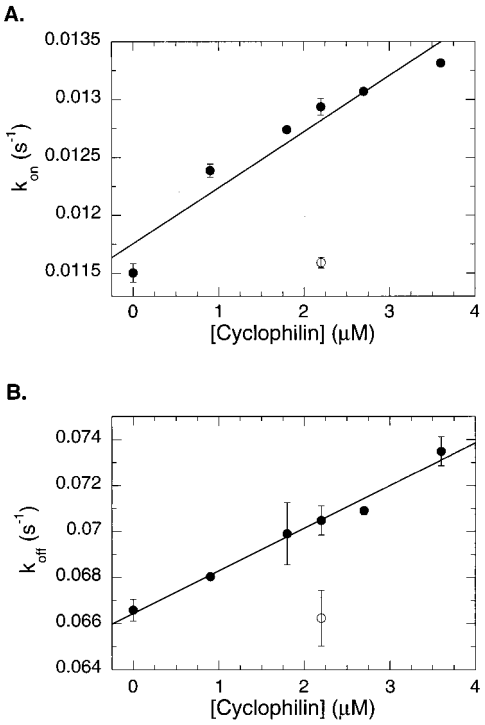


FIGURE 10: Human cyclophilin catalysis of the slow phases of fluorescence change. Rate constants for the slow phase following the addition of 0.5 mM $CaCl_2$ to 3.6 $\mu$M apo-MBP-C (A) and the addition of 1 mM EGTA to the protein equilibrated with $Ca^{2+}$ (B) are plotted versus the amount of human cyclophilin added to the reaction. The rates are fitted to the equation $k = k_{uncat} + k_{cat}/K_M$ [cyclophilin], yielding $k_{cat}/K_M = 550$ $M^{-1}$ $s^{-1}$ and 1820 $M^{-1}$ $s^{-1}$. The open circles represent reactions containing 2.2 $\mu$M cyclophilin plus 5 $\mu$M cyclosporin A.

*Cyclophilin Catalysis of Tryptophan Fluorescence Changes*. Cyclophilins are ubiquitous enzymes which catalyze the isomerization of prolyl peptide bonds in small peptides and exposed protein loops (*47*). The addition of purified *E. coli* and human cyclophilins to MBP-C slightly accelerates both the rate of the slow phase of fluorescence increase upon $Ca^{2+}$ binding and the rate of the slow phase of fluorescence decrease upon chelator addition (Figure 10). The rate acceleration is proportional to the amount of cyclophilin, and in the case of human cyclophilin, the rate acceleration can be nearly fully inhibited by the addition of 5 $\mu$M cyclophilin inhibitor cyclosporin A (Figure 10). These observations are consistent with the proposal that the slow phase is due to proline isomerization.

Addition of an equimolar amount of cyclophilin to MBP-C produces a rate enhancement of only about 20%. Assuming that the $K_m$ for MBP-C as a substrate is in the millimolar range (or higher), as measured for peptide substrates (*48*), the apparent $k_{cat}/K_m$ for the reaction can be estimated by the dependence of the rate of the slow phase on the concentration of the enzyme added. For the human cyclophilin, $k_{cat}/K_m$ is 550 $M^{-1}$ $s^{-1}$ for the on reaction and 1820 $M^{-1}$ $s^{-1}$ for the off reaction. These rate enhancements are at the low end of the range reported for the cyclophilin-catalyzed isomerization of prolyl peptide bonds in partially folded proteins (*49*) and are 2−3 orders of magnitude lower than rate enhancements seen for small peptide substrates (*48*). Inefficient catalysis of proline isomerization in a wide range of proteins has also been attributed to the poor accessibility of prolyl peptide bonds to the rather restrictive active site of cyclophilin (*50*,

*51*). An attempt to dock the prolyl peptide of apo-MBP-C into the active site of human cyclophilin shows that adjacent loop regions clash with surface loops in cyclophilin (*52*). Despite the modest catalysis by cyclophilin of the slow fluorescence change in apo-MBP-C, the specific effects of cyclophilin on the rates of fluorescence changes clearly indicate that prolyl peptide-bond isomerization accompanies both $Ca^{2+}$ binding and release.

## DISCUSSION

*Structural Basis of Kinetic Observations*. The kinetic measurements reported in this paper suggest that a slow, unimolecular prolyl peptide-bond isomerization event precedes the binding of $Ca^{2+}$ to apo-MBP-C. Likewise, the removal of $Ca^{2+}$ from MBP-C is followed by a slow, prolyl peptide-bond isomerization. The mechanistic schemes that are required to explain these observations can be interpreted most clearly by reference to the structural observations reported in the previous paper (*14*).

Model 2 in Figure 6B best describes the data presented here and explains all kinetic observations at physiologically relevant concentrations of $Ca^{2+}$ (i.e., less than or equal to 1 mM). This scheme invokes a slow isomerization reaction between the two states $C_0$ and $T_0$, which may be interpreted as alternative forms of the apoprotein containing either a cis or trans peptide bond, respectively, preceding $Pro^{191}$, as observed in the crystal structure of $Ca^{2+}$-free MBP-C (Figure 2C,D; also see ref *14*). The slow rate of interconversion between these two species and the large enthalpy of activation associated with the interconversion reactions are consistent with the structural interpretation that a cis−trans prolyl peptide isomerization reaction occurs during the interconversion between the two states. Although none of the crystallographically determined structures corresponds to $C_1$ (a 1-$Ca^{2+}$ form with $Pro^{191}$ in the cis conformation), this is a physically reasonable intermediate state, probably similar in structure to either $C_0$ or $C_2$, but with one $Ca^{2+}$ bound to either $Ca^{2+}$ site 1 or 2. $C_2$ corresponds to the two-$Ca^{2+}$ form with $Pro^{191}$ in the cis conformation (Figure 2a), a structure seen in many $Ca^{2+}$- or lanthanide-saturated MBP crystal strutures (*5*−*7*, *11*, *43*, *53*). The structural data show that the conformation of the main chain around $Pro^{191}$ in $C_0$ (and presumably $C_1$) is essentially the same as in $C_2$, but the side chains of $Glu^{190}$ and $Asn^{192}$ differ from their conformations in $C_2$ by one or two side chain torsion angles (*14*). In contrast, the main chain conformations of this loop and the following loop (loops 3 and 4; see preceding paper (*14*)) in $T_0$ differ dramatically from those of $C_2$. In particular, the side chains of both $Glu^{190}$ and $Asn^{192}$ are rotated nearly 180° about the main chain, resulting in a displacement of over 10 Å.

The structural observations also suggest explanations for the burst and slow phases of the kinetics, as well as the variation in rate of the slow phase as a function of the amount of added $Ca^{2+}$. The burst phase corresponds to the conversion of $C_0$ to $C_1$ or $C_2$ and is not limited in rate by the isomerization of peptide bonds. According to this interpretation, $C_0$ is the form of the apoprotein primed for binding to $Ca^{2+}$ by the presence of the cis peptide bond preceding $Pro^{191}$. The structural transitions required for $Ca^{2+}$ binding thus occur with the fast kinetics of a process for which the rate is determined by the relatively small conformational changes accompanying the rotation of side chain and main chain torsion angles about single bonds. In contrast, molecules of apoprotein with a trans peptide bond preceding $Pro^{191}$ must undergo large conformational changes, including a 180° rotation about a peptide bond, before being able to bind to $Ca^{2+}$.

The variation in rate as a function of the amount of added $Ca^{2+}$ suggests that the binding of $Ca^{2+}$ involves a sequence of two reactions, in which the rate of the second, slow reaction is dependent on the concentration of $Ca^{2+}$. As the concentration of $Ca^{2+}$ is raised (up to at least 1 mM), the rate constant of the slow phase following $Ca^{2+}$ binding decreases (Figure 4A). The mechanisms presented in models 1 and 2 (Figure 6A,B) indicate that the relaxation rate constant for the slow cis−trans isomerization equilibrium is the sum of the forward and backward rate constants (eq 3a). The contribution of the backward rate constant to the overall rate constant decreases at high concentrations of $Ca^{2+}$, because higher amounts of $Ca^{2+}$ lead to the depletion of the intermediate $C_0$ during the course of the reaction. Therefore, at high concentrations of $Ca^{2+}$, the relaxation rate constant of the slow phase approaches the limiting value of the forward rate constant. The quantitative agreement between this mechanism and the experimental data is excellent (Figure 7).

Model 2 is an attractive minimal mechanism that can account for the behavior of the system at physiologically relevant concentrations of $Ca^{2+}$. The kinetics of fluorescence changes above 1 mM $Ca^{2+}$, however, cannot be explained by this mechanism (Figure 7). Moreover, the structure of the one-$Ho^{3+}$ form of MBP-A (Figure 2B; ref *14*) indicates that a form of the protein containing a single divalent cation bound to site 1 and a trans peptide preceding $Pro^{191}$ is significantly populated at intermediate concentrations of $Ho^{3+}$ and perhaps also $Ca^{2+}$, and this state does not correspond to any of the states in model 2.

Two slightly more complex models can account for both of the deficiencies of the simpler model. Model 3 introduces state $T_1$, which corresponds to a one-$Ca^{2+}$ form of the protein with a trans peptide preceding $Pro^{191}$. It is likely that this kinetic intermediate represents a conformation similar to that observed in the crystallographically observed one-$Ho^{3+}$-form of MBP-A (Figure 2B). Adding this state to the model allows for an alternative $Ca^{2+}$-binding pathway, which becomes important at high concentrations of $Ca^{2+}$, and can account for the increase in the rate of the slow phase when more than 1 mM $Ca^{2+}$ is added (Figure 4A). The residual plot, however, reveals remaining systematic deviations (Figure 7). A six-state model introducing state $T_2$, perhaps corresponding to a two-$Ca^{2+}$ form of the protein with a trans peptide preceding $Pro^{191}$, reduces some of these deviations. Unfortunately, the increased complexity of the five- and six-state models introduces parameters which are not well-defined by the experiments presented in this paper. These models merely suggest simple and physically plausible explanations for the behavior of the system at high concentrations of $Ca^{2+}$, and other models of similar or greater complexity may account for the observed kinetics equally well. Several other mechanisms have also been considered, but these tend to fit the data more poorly or else invoke larger numbers of parameters. For example, models involving parallel random addi-

tion pathways for $Ca^{2+}$ binding, with intermediates containing one $Ca^{2+}$ bound to either site 1 or site 2, do not fit the data as well as the equally complex five- and six-state schemes presented in models 3 and 4.

A limitation of the kinetic models described in Figure 6 and the results presented in Table 1 is that several of the parameters are highly correlated when fit to the data reported here. For example, because the time scale of the kinetic measurements is too coarse, the forward and backward rate constants for each equilibrium involving the binding and release of $Ca^{2+}$ are highly correlated, and only the ratios of these rate constants are well-defined (eq 3b). The bimolecular rate constants for the $Ca^{2+}$-binding steps have been set to $10^6$ $M^{-1}$ $s^{-1}$ during parameter optimization, because the kinetics predicted by the model over the time scale of the experiments are not sensitive to this parameter unless the rate constant is reduced below $10^5$ $M^{-1}$ $s^{-1}$, at which point the bimolecular $Ca^{2+}$-binding step becomes rate-limiting at low concentrations of $Ca^{2+}$. A value in the range $10^6-10^8$ $M^{-1}$ $s^{-1}$ for the bimolecular rate constant is comparable to experimentally determined rate constants for $Ca^{2+}$-binding reactions in a number of proteins (*42*). Stopped-flow experiments are needed to define precisely the kinetics of the faster $Ca^{2+}$-binding steps in the MBPs, but for the purposes of analyzing the much slower isomerization steps, the approximations used in this paper are acceptable. A second limitation of the modeling is that the molar fluorescence values of the more poorly populated intermediate states present in the more complex models are highly correlated with the rate constants of steps involving these species. Additional experiments at higher concentrations of $Ca^{2+}$, double-mixing experiments, and stopped-flow experiments would help to define the molar fluorescence value of the poorly populated intermediates $T_1$ and $T_2$, as well as the rate constants involving the formation and removal of these intermediates.

Despite these limitations, the global analysis of binding kinetics in terms of models 1−4 indicate that the parameters describing the slow steps are well-determined by the experiments reported here. Most importantly, the unimolecular isomerization rate constants for the interconversion of $C_0$ and $T_0$ are not highly correlated with other parameters. These rate constants are well-defined, because the equilibrium ratio of $C_0$ and $T_0$, and the kinetics following the addition of chelator to the $Ca^{2+}$-saturated protein are both determined directly by these two rate constants (eq 3). Moreover, both the rate constants and amplitudes of the slow phase following the addition of $Ca^{2+}$ are sensitive to these rate constants (eq 3b). The ratio of the forward and backward rate constants for the equilibrium between $T_0$ and $C_0$ refines to a value between 4 and 5 (Table 1), which corresponds to 80−85% of the apoprotein adopting the trans conformation.

*Functional Implications of cis−trans Prolyl Peptide Isomerization Accompanying $Ca^{2+}$ Binding in C-type Animal Lectins*. Structure-based sequence alignments indicate that the $Ca^{2+}$- and carbohydrate-binding site containing the cis-proline in the MBPs is highly conserved in all C-type lectins that are known to bind carbohydrates (*10*, *54*, *55*). Because the tripeptide sequence containing the cis-proline is an integral part of this binding site, isomerization of the proline like that observed in the MBPs may accompany the binding of $Ca^{2+}$ in a wide range of C-type lectins. In turn, the existence of a prolyl peptide isomerization event accompanying $Ca^{2+}$ binding implies that the kinetics of $Ca^{2+}$ binding in many C-type lectins may show hysteresis; that is, the overall rate of $Ca^{2+}$ binding will reflect the previous conformational state of the apoprotein. If the proline in the apoprotein remains in the cis conformation, the binding of $Ca^{2+}$ would be limited in rate by the relatively fast bimolecular reaction between protein and metal ion, but if the proline isomerizes to the trans conformation, the binding of $Ca^{2+}$ would be limited in rate by the relatively slow isomerization reaction. The fact that the proline in 80−85% of the apoprotein molecules is in the trans form suggests that proline isomerization will have a significant effect on the overall kinetics of $Ca^{2+}$ binding in the C-type lectins.

The slow kinetics of $Ca^{2+}$ binding may have an essential role in receptor-mediated endocytosis. Several C-type lectins, including the hepatic lectins (asialoglycoprotein receptors), the macrophage galactose receptor, and the macrophage mannose receptor, undergo internalization and recycling to the cell surface (*1*). During this process, a carbohydrate-bearing ligand is bound by the lectin at the cell surface, and the lectin−ligand complex is internalized in an endocytic vesicle. Acidification of the vesicle titrates the $Ca^{2+}$ off the protein, causing the ligand to dissociate from the lectin. The ligand and membrane-bound lectin are sorted into different vesicles, and the lectin is recycled back to the cell surface (*56*). This process is essential for the internalization of glycoprotein ligands into hepatocytes and macrophages, and relies on the efficient pH-coupled release and rebinding of ligands by the $Ca^{2+}$-dependent lectin (*57*). The kinetics of receptor recycling in a cell occurs on a time scale comparable to that of protein conformational changes governed by proline isomerization. Recycling of the asialoglycoprotein receptor in a hepatoma cell line can be divided into a phase involving ligand binding whose rate is dependent on the concentrations of receptor and ligand, and a phase dependent only on the mechanics of endocytosis and vesicle sorting (*58*). The first phase has a half-life of 8.7 min in the presence of a half-saturating concentration of ligand, whereas the second phase requires roughly 6 min to complete at 37 °C.

A peptide isomerization event following the loss of $Ca^{2+}$ may have two effects that are relevant on the time scale of the endocytic cycle. First, the receptor may remain in the $Ca^{2+}$-free state for one or two minutes, which is long enough for a significant fraction of the receptor molecules to isomerize into a form ($T_0$ in models 1−4, Figure 6) that cannot bind either $Ca^{2+}$ or carbohydrate ligands. In this case, the receptor would be kinetically trapped in a binding-incompetent state to facilitate its separation from the carbohydrate ligand. Second, once the receptor is brought into a neutral pH environment with sufficient $Ca^{2+}$, there will be a lag phase with a half-life on the order of one or two minutes in the activation of those molecules which have isomerized to the $T_0$ state. This trans to cis isomerization event would be the kinetic penalty required to pay for the first isomerization event. Although the measurements reported here were made at neutral pH, the kinetics of proline isomerization is not strongly dependent on pH in the range 5.0−7.5 (*17*), which is the range of pH that various receptors are likely to encounter during the endocytic cycle.

The measurements reported in this paper were performed on a protein not known to participate in receptor-mediated

endocytosis. C-type lectins that participate in endocytosis may have evolved specific mechanisms to modify the kinetics of conformational changes to optimize the benefits of proline isomerization and minimize the penalties. Further experiments will be needed to assess the role of proline isomerization in those C-type lectins that are known to function as endocytic receptors.

## ACKNOWLEDGMENT

We thank Lubert Stryer for generously providing access to his fluorimeter; Jim Ames for helpful advice throughout the course of this work; Audrey Gasch for conducting early experiments on the binding of $Ca^{2+}$ to MBP-A and making the initial discovery of a slow, $Ca^{2+}$-dependent fluorescence change; and Chris Walsh and Barry Nall for sending us plasmids and strains for the expression of *E. coli* and human cyclophilins. Finally, we gratefully acknowledge Suzanne Admiraal, Anne Baldwin, Robert Baldwin, Kurt Drickamer, Daniel Herschlag, Sabine Pokutta, and Sigurd Wilbanks for helpful comments on the manuscript.

## REFERENCES

1. Drickamer, K., and Taylor, M. E. (1993) *Annu. Rev. Cell Biol. 9*, 237−264.
2. Drickamer, K., Dordal, M. S., and Reynolds, L. (1986) *J. Biol. Chem. 261*, 6878−6886.
3. Sastry, K., Zahedi, K., Lelias, J.-M., Whitehead, A. S., and Ezekowitz, R. A. B. (1991) *J. Immunol. 147*, 692−697.
4. Mogues, T., Ota, T., Tauber, A. I., and Sastry, K. N. (1996) *Glycobiology 6*, 543−550.
5. Weis, W. I., Kahn, R., Fourme, R., Drickamer, K., and Hendrickson, W. A. (1991) *Science 254*, 1608−1615.
6. Weis, W. I., Drickamer, K., and Hendrickson, W. A. (1992) *Nature 360*, 127−134.
7. Ng, K. K.-S., Drickamer, K., and Weis, W. I. (1996) *J. Biol. Chem. 271*, 663−674.
8. Kolatkar, A. R., and Weis, W. I. (1996) *J. Biol. Chem. 271*, 6679−6685.
9. Ng, K. K.-S., and Weis, W. I. (1997) *Biochemistry 36*, 979−988.
10. Drickamer, K. (1992) *Nature 360*, 183−186.
11. Sheriff, S., Chang, C. Y., and Ezekowitz, R. A. B. (1994) *Nat. Struct. Biol. 1*, 789−794.
12. Graves, B. J., Crowther, R. L., Chandran, C., Rumberger, J. M., Li, S., Huang, K.-S., Presky, D. H., Familletti, P. C., Wolitzky, B. A., and Burns, D. K. (1994) *Nature 367*, 532−538.
13. Nielsen, B. B., Kastrup, J. S., Rasmussen, H., Holtet, T. L., Graversen, J. H., Etzerodt, M., Thogersen, H. C., and Larsen, I. K. (1997) *FEBS Lett. 412*, 388−396.
14. Ng, K. K.-S., Park-Snyder, S., and Weis, W. I. (1998) *Biochemistry 37*, 17965−17976.
15. Kim, P. S., and Baldwin, R. L. (1982) *Annu. Rev. Biochem. 51*, 459−489.
16. Grathwohl, C., and Wuthrich, K. (1981) *Biopolymers 20*, 2623−2633.
17. Stein, R. L. (1993) *Adv. Protein Chem. 44*, 1−24.
18. Evans, T. C., Jr., and Nelsestuen, G. L. (1996) *Biochemistry 35*, 8210−8215.
19. Sheng, X. R., Zhang, H. J., Pan, X. M., Li, X. F., and Zhou, J. M. (1997) *FEBS Lett. 413*, 429−432.
20. Auld, D. S. (1988) *Methods Enzymol. 158*, 13−14.
21. Weis, W. I., Crichlow, G. V., Murthy, H. M. K., Hendrickson, W. A., and Drickamer, K. (1991) *J. Biol. Chem. 266*, 20678−20686.
22. Burrows, L., Iobst, S. T., and Drickamer, K. (1997) *Biochem. J. 324*, 673−680.
23. Fornstedt, N., and Porath, J. (1975) *FEBS Lett. 57*, 187−191.
24. Gill, S. C., and von Hippel, P. H. (1989) *Anal. Biochem. 182*, 319−326.
25. Bates, R. G., and Hetzer, H. B. (1961) *J. Chem. Soc. 1961*, 667−671.
26. Good, N. E., Winget, G. D., Winter, W., Connolly, T. N., Izawa, S., and Singh, R. M. M. (1966) *Biochemistry 5*, 467−477.
27. Tsien, R., and Pozzan, T. (1989) *Methods Enzymol. 172*, 230−263.
28. Liu, J., and Walsh, C. T. (1990) *Proc. Natl. Acad. Sci. U.S.A. 87*, 2304−2308.
29. Liu, J., and Walsh, C. T. (1990) *Proc. Natl. Acad. Sci. U.S.A. 87*, 4028−4032.
30. Marquardt, D. W. (1963) *J. Soc. Ind. Appl. Math. 11*, 431−441.
31. Barshop, B. A., Wrenn, R. F., and Frieden, C. (1983) *Anal. Biochem. 130*, 134−145.
32. Mendes, P. (1997) *Trends Biochem. Sci. 22*, 361−363.
33. Zimmerle, C., and Frieden, C. (1989) *Biochem. J. 258*, 381−387.
34. Andersen, T. T., Freytag, J. W., and Hill, R. L. (1982) *J. Biol. Chem. 257*, 8036−8041.
35. Haagsman, H. P., Sargeant, T., Hauschka, P. V., Benson, B. J., and Hawgood, S. (1990) *Biochemistry 29*, 8894−8900.
36. Ewart, K. V., Yang, D. S. C., Ananthanarayanan, V. S., Fletcher, G. L., and Hew, C. L. (1996) *J. Biol. Chem. 271*, 16627−16632.
37. Eigen, M., and De Maeyer, L. (1963) in *Technique of Organic Chemistry* (Friess, S. L., Lewis, E. S., and Weissberger, A., Eds.) pp 895−1054, Wiley-Interscience, New York.
38. Connors, K. A. (1990) *Chemical Kinetics*, VCH, New York.
39. Hagerman, P. J., and Baldwin, R. L. (1976) *Biochemistry 15*, 1462−1473.
40. Naraghi, M. (1997) *Cell Calcium 22*, 255−268.
41. Wu, S. L., Johnson, K. A., and Horrocks, W. D., Jr., (1997) *Inorg. Chem. 36*, 1884−1889.
42. Falke, J. J., Drake, S. K., Hazard, A. L., and Peersen, O. B. (1994) *Q. Rev. Biophys. 27*, 219−290.
43. Burling, F. T., Weis, W. I., Flaherty, K. M., and Brünger, A. T. (1996) *Science 271*, 72−77.
44. Horrocks, W. D., and Sudnick, D. R. (1981) *Acc. Chem. Res. 14*, 384−392.
45. Levitt, M. (1981) *J. Mol. Biol. 145*, 251−263.
46. Jullien, M., and Baldwin, R. L. (1981) *J. Mol. Biol. 145*, 265−280.
47. Schmid, F. X. (1998) in *Molecular chaperones in the life cycle of proteins* (Fink, A. L., and Goto, Y., Eds.) pp 361−389, Marcel Dekker, New York.
48. Kofron, J. L., Kuzmic, P., Kishore, V., Colon-Bonilla, E., and Rich, D. H. (1991) *Biochemistry 30*, 6127−6134.
49. Veeraraghavan, S., Nall, B. T., and Fink, A. L. (1997) *Biochemistry 36*, 15134−15139.
50. Lang, K., Schmid, F. X., and Fischer, G. (1987) *Nature 329*, 268−270.
51. Lin, L.-N., Hasumi, H., and Brandts, J. F. (1988) *Biochim. Biophys. Acta 956*, 256−266.
52. Taylor, P., Husi, H., Kontopidis, G., and Walkinshaw, M. D. (1997) *Prog. Biophys. Mol. Biol. 67*, 155−181.
53. Weis, W. I., and Drickamer, K. (1994) *Structure 2*, 1227−1240.
54. Drickamer, K. (1993) *Prog. Nucleic Acid Res. Mol. Biol. 45*, 207−232.
55. Day, A. J. (1994) *Biochem. Soc. Trans. 22*, 83−88.
56. Schwartz, A. L. (1995) *Pediatr. Res. 38*, 835−843.
57. Loeb, J. A., and Drickamer, K. (1988) *J. Biol. Chem. 263*, 9752−9760.
58. Schwartz, A. L., Fridovich, S. E., and Lodish, H. F. (1982) *J. Biol. Chem. 257*, 4230−4237.

BI9819733